J. Fluid Mech. (2008), *vol.* 597, *pp.* 283–303.
doi:10.1017/S0022112007009780 Printed in the United Kingdom

Inviscid waves on a Lamb–Oseen vortex in a rotating stratified fluid: consequences for the elliptic instability

STÉPHANE LE DIZÈS

Institut de Recherche sur les Phénomènes Hors Équilibre, CNRS,
49, rue F. Joliot-Curie, BP 146, F-13384 Marseille cedex 13, France

(Received 30 March 2007 and in revised form 19 October 2007)

The inviscid waves propagating on a Lamb–Oseen vortex in a rotating medium for an unstratified fluid and for a strongly stratified fluid are analysed using numerical and asymptotic approaches. By a local Lagrangian description, we first provide the characteristics of the local plane waves (inertia–gravity waves) as well as the local growth rate associated with the centrifugal instability when the vortex is unstable. A global WKBJ approach is then used to determine the frequencies of neutral core modes and neutral ring modes. We show that these global Kelvin modes only exist in restricted domains of the parameters. The consequences of these domain limitations for the occurrence of the elliptic instability are discussed. We argue that in an unstratified fluid the elliptic instability should be active in a small range of the Coriolis parameter which could not have been predicted from a local approach. The wavenumbers of the sinuous modes of the elliptic instability are provided as a function of the Coriolis parameter for both an unstratified fluid and a strongly stratified fluid.

1. Introduction

Waves on vortices have been known for many years to be responsible for several rich dynamical behaviours. They can be the source of strong nonlinear phenomena when they interact, leading sometimes to vortex bursting. They can be resonantly excited by the background flow as in the elliptical instability. The purpose of this work is to provide some information on these waves for a smooth vortex in a rotating and stratified fluid. The paper focuses on a vortex with a Gaussian vorticity profile (the Lamb–Oseen vortex), but the analysis can be applied to any other vortex.

Fabre, Sipp & Jacquin (2006) have provided a comprehensive study of the linear viscous waves propagating on a Lamb–Oseen vortex in a unstratified and non-rotating fluid. They have shown that the Lamb–Oseen vortex possesses different types of waves, characterized by their structure, direction of propagation and damping rate. In particular, they were able to show that the inviscid Kelvin waves which were known to exist in a Rankine vortex were also present in the viscous spectrum of the Lamb–Oseen vortex in the frequency range where there is no critical point. These inviscid waves have also been studied by a WKBJ method in Le Dizès & Lacaze (2005) for arbitrary vortex profiles. Le Dizès & Lacaze (2005) have shown that, for small azimuthal wavenumbers, their frequencies can be obtained with good precision by an asymptotic formula expressing that the eigenfunction exhibits a discretized

number of radial oscillations in the vortex core. A similar theory will be used here in the framework of rotating and stratified fluids.

The effect of stratification on the inviscid spectrum of axisymmetrical waves for the Lamb–Oseen vortex has been analysed by Miyazaki & Fukumoto (1991). They have shown that no axisymmetrical wave exists when the fluid is strongly stratified. We shall see here that axisymmetrical waves may exist if the vortex is in an anticyclonic rotating environment.

A Lamb–Oseen vortex in a rotating environment can become unstable by the centrifugal instability. The characteristic features of this instability have been known for many years (see Drazin & Reid 1981). The instability mode is stationary ($\omega = 0$) and axisymmetric ($m = 0$). The instability mechanism is inviscid and a necessary condition for instability is that the local generalized Rayleigh discriminant becomes negative (Kloosterziel & van Heijst 1991; Billant & Gallaire 2005). The centrifugal instability is also active in a stably stratified fluid (Billant & Gallaire 2005), but stratification tends to inhibit the axisymmetric centrifugal mode (Withjack & Chen 1974; Boubnov, Gledzer & Hopfinger 1995). For general vortices, the centrifugal instability can be in competition with other instabilities such as the shear instability (e.g. Afanasyev & Peltier 1998) or the elliptical instability if the vortex is in a non-axisymmetrical environment (Afanasyev 2002). However, the Lamb–Oseen vortex is not affected by the shear instability (Saffman 1992).

The elliptical instability has been studied in detail for an unstratified non-rotating fluid (Kerswell 2002). For a Lamb–Oseen vortex, the most unstable mode has been shown to be a stationary sinuous mode corresponding to the combination of two helical Kelvin modes $m = 1$ and $m = -1$. The selected axial wavenumber depends on the Kelvin mode characteristics while the instability growth rate is apparently predicted well by a local estimate calculated from the characteristics of the vortex near its centre only (Le Dizès & Laporte 2002). Such a local estimate for the instability growth rate is based on an inertial wave decomposition (Bayly 1986; Waleffe 1990). The effects of background rotation and stratification on this estimate have already been calculated (Craik 1989; Miyazaki & Fukumoto 1992; Miyazaki 1993). In particular, it has been shown that anticyclonic rotation can stabilize the elliptic instability in an unstratified fluid for a specific range of Coriolis parameters (Craik 1989; Le Bars, Le Dizès & Le Gal 2007) while strong stratification can be destabilizing in the same Coriolis parameter range (Leblanc 2003). However, very few results are known on the instability when the global geometry of the flow is taken into account. In a rotating but non-stratified fluid, Afanasyev (2002) demonstrated experimentally that the elliptic instability was active in the weakly anticyclonic vortex of a vortex pair. A similar observation was made by Stegner, Pichon & Beunier (2005) in the anticyclonic vortices of a Bénard–von Kármán vortex street. Le Bars *et al.* (2007) have considered the flow inside a rotating cylinder. They have analysed how the finite radial and axial extents of the flow select the global Kelvin modes involved in the instability when the Coriolis parameter is modified. In that case, the flow is uniform and there are no critical layers and they have been able to show that the local instability approach provides a very good estimate for the instability growth rate.

When the vortex has a non-uniform vorticity profile, the local approach does not always provide relevant results. The main reason comes from the presence of critical points which damp some of the global modes. As the elliptic instability results from the resonance of neutral global Kelvin modes, when the global modes become damped, the elliptic instability disappears. This phenomenon explains the stabilization

of the sinuous mode of the elliptic instability for a Lamb–Oseen vortex when a weak axial flow is added (Lacaze, Ryan & Le Dizès 2007). It also probably explains the stabilization of this mode when a weak stratification is added, as observed for co-rotating vortex pairs (Otheguy, Chomaz & Billant 2006*b*).

In the present paper, we shall obtain the characteristics of global Kelvin modes when the Coriolis parameter is varied in an unstratified fluid and in a strongly stratified fluid and provide new necessary conditions for the occurrence of the elliptic instability.

It has been discovered that in a strongly stratified fluid, two interacting vortices can also be made unstable by another instability called the zigzag instability (see Billant & Chomaz 2000*a–c*). This instability, whose wavelength scales with the distance between the two vortices, is the analogue of the Crow instability affecting counter-rotating vortices in an unstratified fluid (Crow 1970). In a strongly stratified fluid, it also affects co-rotating vortex pairs (Otheguy *et al.* 2006*a*, *b*). This instability can be linked to the coupling of the translating modes of each vortex (Billant, Chomaz & Otheguy 2005). Because these modes are mainly two-dimensional (their wavelength is much larger than the vortex core size), we will not be able to capture them by our analysis which uses a large-wavenumber approach.

The paper is organized as follows. In § 2, the local stability properties of an axisymmetrical vortex in a rotating and stratified fluid are provided. The centrifugal instability criterion is recovered. The local stability properties of a Lamb–Oseen vortex are determined. The characteristics of neutral inertia gravity waves are also provided. In § 3, the asymptotic approach used to describe the global Kelvin modes is briefly presented and is applied to the Lamb–Oseen vortex. The frequency range of the global Kelvin modes is determined as a function of the Coriolis parameter for different azimuthal wavenumbers in the unstratified and strongly stratified cases. In the last section, the consequences of the global Kelvin mode characteristics on the elliptical instability are discussed. The evolution of the axial wavenumber of the sinuous modes is in particular determined as the Coriolis parameter is varied for the unstratified case and the strongly stratified case.

2. Framework and local stability properties

We consider a stationary axisymmetrical vortex of angular velocity $\Omega_0(r)\boldsymbol{e}_z$ with

$$\Omega_0(r) = \frac{1-\exp(-r^2)}{r^2}, \tag{2.1}$$

in a fluid rotating at the angular velocity $f\boldsymbol{e}_z$ and linearly stratified along the vortex axis with a constant Brunt–Väisälä frequency $N = \sqrt{-g\partial_z\rho_0/\rho_0}$. Viscous diffusion of the vortex is neglected. All the variables are non-dimensionalized using the maximum angular velocity, the core size of the vortex, and the mean density of the fluid. Note that, with our normalization, the Rossby and Froude numbers are $Ro = 2/f$ and $Fr = 2/N$, respectively.

In an inviscid and Boussinesq framework, the linear perturbations of velocity $\boldsymbol{u}$, pressure p and density ρ are governed by the system of equations:

$$\frac{\partial \boldsymbol{u}}{\partial t} + (\boldsymbol{U}_0\cdot\nabla)\boldsymbol{u} + (\boldsymbol{u}\cdot\nabla)\boldsymbol{U}_0 + 2f\boldsymbol{e}_z\times\boldsymbol{u} = -\nabla p - N^2\rho\boldsymbol{e}_z, \tag{2.2a}$$

$$\frac{\partial \rho}{\partial t} + (\boldsymbol{U}_0\cdot\nabla)\rho - \boldsymbol{u}\cdot\boldsymbol{e}_z = 0, \tag{2.2b}$$

$$\nabla\cdot\boldsymbol{u} = 0, \tag{2.2c}$$

where $\boldsymbol{U}_0 = (0, r\Omega_0(r), 0)$ is the vortex velocity field in cylindrical coordinates in the rotating frame.

The goal of the present paper is to obtain information on the linear perturbations, especially their frequency. We now first analyse the local stability characteristics of the perturbations using the Lagrangian approach developed by Lifschitz & Hameiri (1991). In this framework, the local stability properties of the vortex are obtained by considering local plane wave solutions

$$(\boldsymbol{u}, p, \rho) = (\boldsymbol{u}_l, p_l, \rho_l)\exp(\mathrm{i}\boldsymbol{k}\cdot\boldsymbol{x}) \tag{2.3}$$

along a streamline trajectory of the vortex in the limit of large $|\boldsymbol{k}|$ (Lifschitz & Hameiri 1991; Friedlander & Lipton-Lifschitz 2003). In this limit, the phase factor $\boldsymbol{k}\cdot\boldsymbol{x}$ is found to be conserved along the fluid trajectories and $\boldsymbol{k}$ is given on the fluid trajectory $\boldsymbol{x} = (r\cos(\Omega_0(r)t), r\sin(\Omega_0(r)t), z)$ by

$$\boldsymbol{k} = (k\cos\theta\cos(\Omega_0(r)t), k\cos\theta\sin(\Omega_0(r)t), k\sin\theta), \tag{2.4}$$

where the inclination angle θ and the wavevector amplitude $k = |\boldsymbol{k}|$ are constants. The perturbation amplitudes are found to satisfy an equation which admits solutions varying as $\exp(\mathrm{i}\omega_l t)$ provided that the local frequency ω_l satisfies the relation

$$\omega_l^2 = 2(\Omega_0 + f)(\zeta_0 + 2f)\cos^2\theta + N^2\sin^2\theta, \tag{2.5}$$

where $\zeta_0(r) = 2\Omega_0(r) + r\Omega_0'(r)$ is the vorticity of the vortex. The absolute vorticity is then $\zeta_0(r) + 2f$. The frequency ω_l is a 'Lagrangian' frequency. It provides the frequency in the frame moving with the fluid particle, that is rotating at the angular velocity $\Omega_0(r) + f$. The relation (2.5) is well-known in the context of uniformly rotating flows as it corresponds to the dispersion relation of inertia-gravity waves (see Staquet & Sommeria 2002). In a non-uniformly rotating flow, (2.5) extends the inertia–gravity wave relation but is valid only locally as both Ω_0 and ζ_0 depend on the radial coordinate r.

Equation (2.5) provides the Rayleigh criterion for centrifugal instability which states that

$$2(\Omega_0(r) + f)(\zeta_0(r) + 2f) < 0 \tag{2.6}$$

is a necessary and sufficient condition for inviscid instability. From (2.5), we can deduce that the local wave whose wavevector is perpendicular to the rotation axis ($\theta = 0$) has a growth rate which is given by

$$\sigma_l = \sqrt{-2(\Omega_0(r) + f)(\zeta_0(r) + 2f)} \tag{2.7}$$

on the streamlines where the Rayleigh criterion is satisfied.

For the Lamb–Oseen vortex, there exists a streamline where the Rayleigh criterion (2.6) is satisfied as soon as the Coriolis parameter f is such that

$$-1 < f < 0. \tag{2.8}$$

For a given streamline, the local maximum growth rate is

$$\sigma_{max}(r) = -\tfrac{1}{2}r\Omega_0'(r), \tag{2.9}$$

which is reached when

$$f = f_{max}(r) \equiv -\big(\Omega(r) + \tfrac{1}{4}r\Omega_0'(r)\big). \tag{2.10}$$

The variations of σ_{max} and f_{max} versus r are given in figure 1(a). For a given Coriolis parameter f, the local stability properties vary from one streamline to the other.

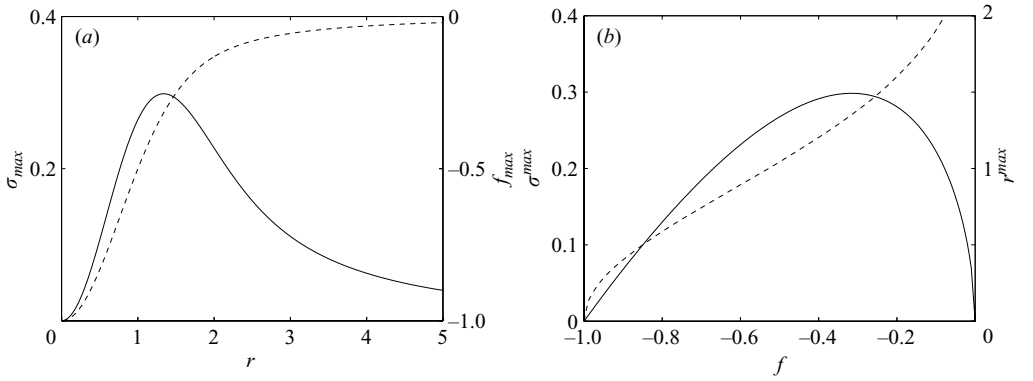

FIGURE 1. Local centrifugal instability growth rate of Lamb–Oseen vortex in a rotating fluid. (*a*) Maximum growth rate (solid line) and most dangerous Coriolis parameter (dashed line) versus the radial coordinate. (*b*) Maximum growth rate (solid line) and most unstable radius (dashed line) versus the Coriolis parameter.

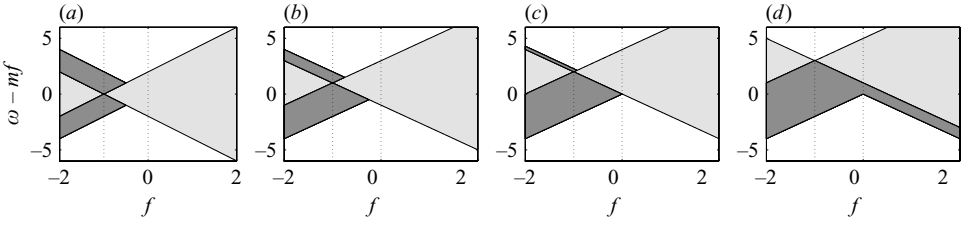

FIGURE 2. Frequency range of the local waves of azimuthal wavenumber m in the rotating frame as a function of the Coriolis parameter f for a unstratified Lamb–Oseen vortex ($N = 0$). (*a*) $m = 0$, (*b*) $m = 1$, (*c*) $m = 2$, (*d*) $m = 3$. Light grey: Frequency range for the waves in the vortex centre only.

The variations of the most unstable radius $r^{max}(f)$ and its corresponding growth rate $\sigma^{max}(f)$ are shown in figure 1(*b*). This figure shows that the centrifugal instability is very strong for small negative values of f. Note in particular that $\sigma > 0.1$ as soon as $-0.85 < f < -0.02$. We therefore expect the centrifugal instability to be a dominant feature of the dynamics of the vortex in almost the whole range of f between -1 and 0.

When f is not in the interval $(-1, 0)$, the Rayleigh criterion is never satisfied and the local Lagrangian frequency ω_l defined by (2.5) is real for all r. If we want to determine the corresponding frequency in a fixed frame, we have to take into account the azimuthal variation of the wave. For instance, if the perturbation amplitude possesses a variation with azimuthal wavenumber m, the frequency of the local wave in a fixed frame would be $\omega = \omega_l + mf + m\Omega_0(r)$.

In figures 2 and 3, we have plotted the domains covered by the local frequencies in the frame rotating at the angular frequency f for $m = 0$ to $m = 3$, for the Lamb–Oseen vortex in the unstratified case and in the strongly stratified case, respectively. To obtain these plots, we have varied the inclination angle from 0 to $\pi/2$ and changed the radial coordinate r. The pale grey regions correspond to the domains covered by the local frequencies for the waves located in the vortex centre ($r = 0$). The white regions indicate the frequency domains which are not accessible by any wave anywhere in the fluid. For instance, we can say from figure 3(*a*) that in a strongly stratified fluid

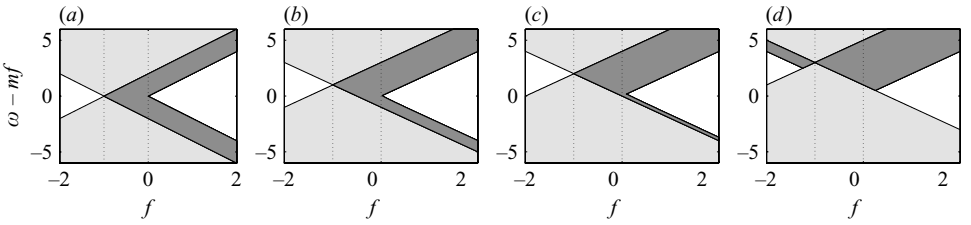

FIGURE 3. Same as figure 2, but for a strongly stratified vortex (large N).

there exist axisymmetrical local waves ($m=0$) of frequency $\omega=1$ for $-3/2<f<1/2$ only, and none are localized in the vortex centre for $-1/2<f<1/2$.

Upon comparing figures 2 and 3, we can see that the frequency domains of the local waves in an unstratified fluid and in a strongly stratified fluid are very different. They are complementary when we consider the local frequency at a given point (in the centre for instance). We can also see that for the Lamb–Oseen vortex, there exist, for all m, local frequencies which can be present in both the unstratified and the strongly stratified case.

Local frequencies are the frequency of local perturbations, that is of perturbations which are sufficiently localized near a given streamline. In the next section, we shall analyse how these frequencies are connected to the frequencies of global mode perturbations. We shall see that when the transverse structure of the perturbation is taken into account, the range of the possible frequencies becomes much smaller.

3. Global Kelvin modes

In this section, we consider linear normal mode perturbations (called global Kelvin modes) of the form

$$(\boldsymbol{u},\, p,\, \rho)=(\boldsymbol{u}_K,\, p_K,\, \rho_K)\exp(\mathrm{i}k_z z+\mathrm{i}m\theta-\mathrm{i}\omega t), \tag{3.1}$$

where k_z and m are axial and azimuthal wavenumbers and ω is the frequency.

The perturbation equations (2.2a)–(2.2c) for such a solution can be reduced to a single equation for the pressure amplitude p_K:

$$\frac{\mathrm{d}^2 p_K}{\mathrm{d}r^2}+\left(\frac{1}{r}-\frac{\Delta_f'}{\Delta_f}\right)\frac{\mathrm{d}p_K}{\mathrm{d}r}+\left(\frac{2m}{r\Phi_f\Delta_f}(\Omega_0'\Delta_f-(\Omega_0+f)\Delta_f')+\frac{k_z^2\Delta_f}{\Phi_f^2-N^2}-\frac{m^2}{r^2}\right)p_K=0, \tag{3.2}$$

where

$$\Phi_f(r)=-\omega+m(\Omega_0(r)+f). \tag{3.3a}$$

$$\Delta_f(r)=2(\zeta_0(r)+2f)(\Omega_0(r)+f)-\Phi_f^2(r). \tag{3.3b}$$

In contrast with local solutions, global Kelvin modes are subject to boundary conditions: p_K must be finite at zero, and must be either an outgoing wave or exponentially small at infinity. These conditions applied to the solutions of (3.2) define the eigenvalue problem for ω (assuming k_z and m are fixed) that we want to solve.

Without stratification and background rotation (that is $N=f=0$), Le Dizès & Lacaze (2005) have shown that, for small m, a good approximation of the dispersion relation and of the eigenmode could be obtained by considering a large k_z asymptotic

approach. We shall see below that the same result is also true in the presence of stratification and background rotation.

The main idea of Le Dizès & Lacaze (2005) is to use a WKBJ approach in which only the term in k_z^2 is retained at leading order in (3.2). This permits us to define a local radial wavenumber $\beta(r)$ given by

$$\beta(r) = k_z \sqrt{\frac{\Delta_f}{\Phi_f^2 - N^2}}. \tag{3.4}$$

The regions where β is real are the regions where the eigenfunction is oscillating. These regions are delimited either by the origin or by a (turning) point where β vanishes. Le Dizès & Lacaze (2005) have shown that core modes (modes localized between the origin and a turning point) and ring modes (modes localized between two turning points) are selected by a condition similar to the Bohr–Sommerfeld quantization rule of quantum mechanics (Landau & Lifchitz 1967). For core modes, this condition reads

$$\int_0^{r_1} \beta(r)\mathrm{d}r = (n + |m|/2)\pi \quad (n = 0, 1, 2\ldots), \tag{3.5}$$

while for ring modes, it is

$$\int_{r_1}^{r_2} \beta(r)\mathrm{d}r = (n + 1/2)\pi \quad (n = 0, 1, 2\ldots), \tag{3.6}$$

where r_1 and r_2 are turning points ($\beta(r_l) = 0$, $l = 1, 2$). These conditions lead to a discretization of the axial wavenumber for fixed m and ω. They also imply that the distance between two consecutive selected axial wavenumbers for fixed m and ω is constant.

The solutions to (3.2) are also known to exhibit critical-point singularities. In a rotating stratified fluid, these singularities occur at the locations where the frequency of the mode in the frame moving with the local angular velocity vanishes or equals the Brunt–Väisälä frequency, that is where $\Phi_f(r) = 0$ or $\Phi_f(r) = \pm N$.

In an unstratified fluid, both types of singularity merge and viscous effects can be added in order to smooth the singularity (Le Dizès 2004). However, an inviscid dispersion relation can still be obtained by integrating (3.2) in the complex r-plane (Sipp & Jacquin 2003). In the WKBJ framework, Le Dizès & Lacaze (2005) have shown that the frequencies of these singular modes were still given by a relation of the form (3.5) or (3.6) but applied in the complex plane. These results were confirmed by Fabre *et al.* (2006) using a viscous code.

Unfortunately, with stratification, very few results are known on the singular global Kelvin modes and we shall not try to analyse the effects of critical-point singularities here. We shall consider only configurations where there is no critical point and such that (3.5) and (3.6) can be applied on the real axis. We shall consider the unstratified case ($N = 0$) and the strongly stratified case (N large) such that the critical-point singularities are associated only with zeros of Φ_f and defined by

$$\omega - mf = \omega_0(r) \equiv m\Omega_0(r). \tag{3.7}$$

The strongly stratified case means that we consider only frequencies such that $-N + m < \omega - mf < N$ (for positive m). When N is large (and m moderate), most frequencies of interest are described by the strongly stratified case. In the Appendix, we briefly discuss how weakly stratified cases can be analysed.

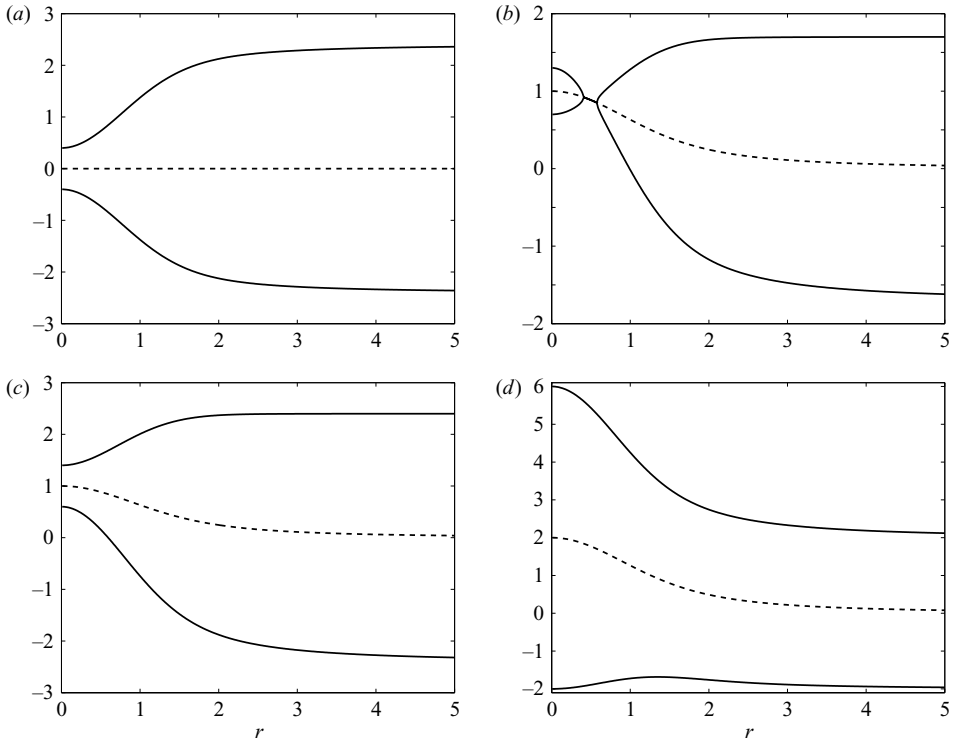

FIGURE 4. Functions $\omega^{\pm}(r)$ (solid lines) and $\omega_0(r)$ (dashed line) versus r. (*a*) $m=0$, $f=-1.2$; (*b*) $m=1$, $f=-0.85$; (*c*) $m=1$, $f=-1.2$; (*d*) $m=2$, $f=1$.

As mentioned above, the existence of core or ring modes is linked to the existence of a finite interval where β is real. In the unstratified case, such an interval corresponds to a region where $\Delta_f > 0$. In the strongly stratified case, it is the opposite: they correspond to a region where $\Delta_f < 0$. The condition of existence of core and ring modes can therefore be analysed easily by locating the zeros of Δ_f which are defined by

$$\omega - mf = \omega^{\pm}(r) \equiv m\Omega_0(r) \pm \sqrt{2(\zeta_0(r) + 2f)(\Omega_0(r) + f)}. \tag{3.8}$$

By plotting the functions $\omega^{\pm}(r)$ and $\omega_0(r)$ versus r, we can easily determine the frequencies in the rotating frame $\omega - mf$ for which Δ_f can change sign. We can then deduce the frequency intervals in which eigenmodes are expected for both unstratified and strongly stratified cases.

Four different examples of variations of ω_0 and $\omega^{\pm}$ are displayed in figure 4. Figure 4(*a*) corresponds to a case with $m=0$ for which there is no critical point. In that case, Δ_f changes sign only if $-2f-2<\omega<-2f$ or $2f<\omega<2f+2$ and for these frequencies, Δ_f is negative between 0 and a turning point r_t, and positive for larger r. It follows that there is no mode in the unstratified case, but there are two frequency intervals $(-2f-2, -2f)$ and $(2f, 2f+2)$ where core modes are expected in the strongly stratified case. This is confirmed in figure 5(*a*) where the frequency of the first global Kelvin modes is plotted versus k_z/N. The numerical results are obtained by a shooting method. It is worth mentioning that the large k_z asymptotic theory provides good estimates for the frequencies up to $k_z=0$. That property, which was

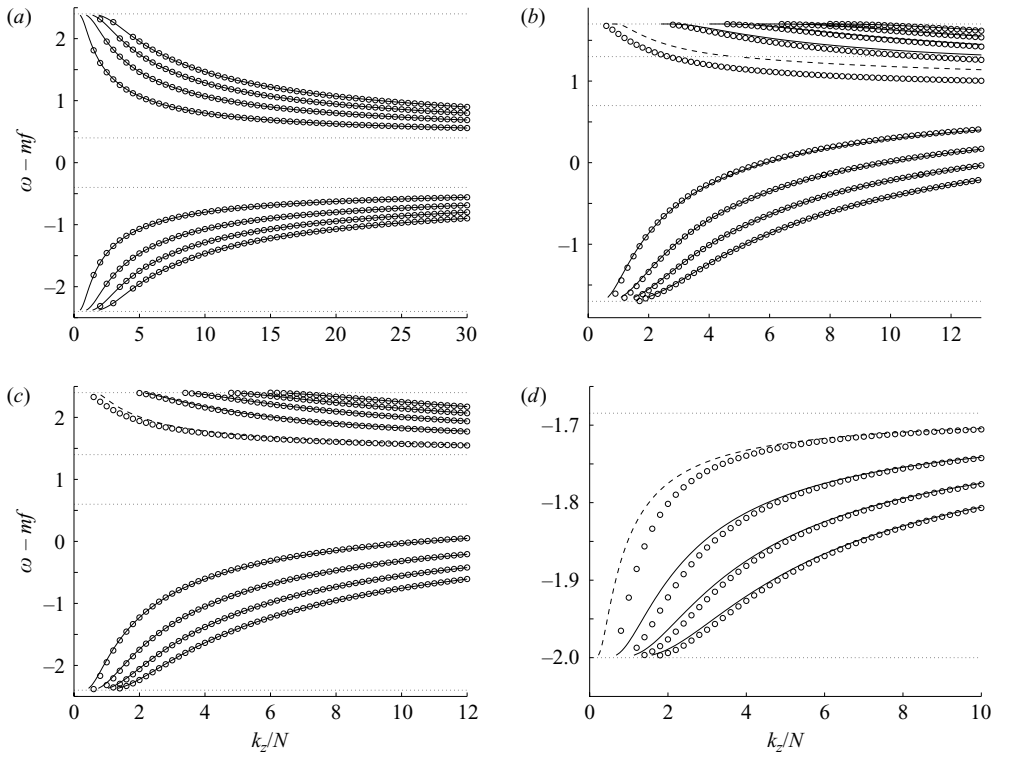

FIGURE 5. Dispersion relation of the first inviscid global Kelvin modes. Solid line, (3.5) or (3.6) with $n \geqslant 1$; dashed line, (3.5) or (3.6) with $n = 0$; symbols, inviscid numerical results. (*a*) $m = 0$, $f = -1.2$, $N = 5$; (*b*) $m = 1$, $f = -0.85$, $N = 5$; (*c*) $m = 1$, $f = -1.2$, $N = 5$; (*d*) $m = 2$, $f = 1$, $N = 5$. In (*b*), the Kelvin modes possess a critical-layer singularity for $0 < \omega < 1$: the numerical modes are (very) slightly damped by this singularity.

already noticed in Le Dizès & Lacaze (2005) for the unstratified non-rotating case, is apparently valid whatever the stratification and the background rotation.

Results for $m = 1$ and $N = 5$ are shown in figures 5(*b*) and 5(*c*) for $f = -0.85$ and $f = -1.2$, respectively. The functions $\omega^{\pm}$ and ω_0 for these two cases are plotted in figures 4(*b*) and 4(*c*). The agreement between the asymptotic formula and the numerics is also good in these cases. In figures 5(b)–5(c), the dashed line corresponds to the asymptotic formula with $n = 0$. This branch is present on the upper side only. The first branch on the lower side starts with the label $n = 1$. This property was also observed in the unstratified non-rotating case for $m = 1$ (Le Dizès & Lacaze 2005) but the branch $n = 0$ was in that case obtained on the lower side only and was associated with the translating mode for $k_z = 0$. It was also remarked that the agreement with the numerics is less good for this branch. For $f = -0.85$ (figures 4*b* and 5*b*), both core modes and ring modes exist. The ring mode frequencies are between 0.7 and 1.3 in the middle interval delimited by dotted lines in figure 5(*b*). For frequencies between 1.3 and 1.7, the eigenmodes are core modes. They exhibit a singular behaviour near $\omega - mf \approx 1.7$: the wavenumbers of all the branches tend to zero. The theory predicts a behaviour like $k_z/N \propto 1/|\log(\delta\omega)|$, which is difficult to capture numerically. Note also that there is a larger discrepancy than in the other cases around the frequency $\omega - mf \approx 1.3$. This frequency corresponds to the change of core modes into ring

modes. Close to this frequency, a turning point is then close to the origin and this was not taken into account in the analysis.

For frequencies between 0 and 1, the eigenmodes exhibit a critical-layer singularity. In the theory, this singularity does not affect the discretization rule. By contrast, this singularity is a problem for the inviscid numerical integration: it must be avoided in the complex plane in the region where the inviscid approximation is expected to be valid. The method is explained in Sipp & Jacquin (2003), for instance. The numerical results shown in figure 5(*b*) for the frequencies in (0, 1) have been obtained by this method. Note that the agreement with the asymptotic formula is also good for these frequencies. The critical-point singularity apparently does not affect the eigenmode selection. Moreover, no significant damping rate has been obtained in the numerics. This could be connected to the property that the critical point is far from the vortex core in a region where the eigenmode is exponentially small.

In figure 5(*d*), results for $m=2$ have been plotted. They correspond to the functions $\omega^{\pm}$ shown in figure 4(*d*). In that case, only ring modes are obtained. Again, all the asymptotic branches are recovered by the numerics. However, the agreement between the numerics and the asymptotic formula is not as good as for the previous cases, especially for small k_z. For larger m, the discrepancies become even more important. As already pointed out in Le Dizès & Lacaze (2005), this can be associated with neglected terms in (3.2) such as m^2/r^2 becoming more important as m increases.

In figure 5, the intervals of frequency obtained from the analysis of the functions $\omega^{\pm}$ in which the asymptotic formula can be applied have been indicated by dotted lines. In all these cases, we have been able to demonstrate that there do exist real eigenmodes in the expected frequency intervals. To prove that there is no eigenmode outside these intervals is by contrast a more difficult problem. We can provide some elements of response in our framework. In particular, we can easily prove (see Le Dizès & Lacaze 2005) that if for a given real frequency, there is no critical point and no finite interval where the radial wavenumber β is real, we cannot construct any eigenmode using the WKBJ framework. This implies that there should not exist neutral modes with such a frequency with a large axial wavenumber. However, we cannot say anything concerning the frequency of the modes with a small axial wavenumber and for which the WKBJ analysis does not apply *a priori*.

When there is a critical point, it is also difficult to conclude anything. We have seen above that a critical-point singularity can have no effect on the dispersion relation of the mode if this singularity is far from the region where the mode is localized. We expect this property to apply in an unstratified fluid. However, Le Dizès & Lacaze (2005) have also shown that when the critical point becomes close to the region of localization of the mode (between 0 and r_1 for the core modes, or between r_1 and r_2 for the ring modes), the mode becomes strongly damped. In a strongly stratified fluid, the critical-layer singularity which is associated with $\Phi_f=0$ has a different nature and its effect is not well known. This singularity is weaker than the critical-point singularity in unstratified fluid as it does not affect the leading-order WKBJ approximation of the eigenmode. Moreover, the numerical simulations of Le Dizès & Billant (2006) tend to show that this singularity could have a weak destabilizing role. Here, we shall not address this issue which is considered in another work (Le Dizès & Billant 2007).

In figures 6 to 9 are indicated, in the $(f, \omega-mf)$-plane, the regions of the parameter where core modes and ring modes are expected for m ranging from 0 to 3 in both the unstratified case (figures 6*a*, 7*a*, 8*a* and 9*a*) and the strongly stratified case (figures 6*b*, 7*b*, 8*b* and 9*b*). The dotted vertical lines located at $f=-1$ and $f=0$ delimit the interval of Coriolis parameters where the centrifugal instability is active. The dotted

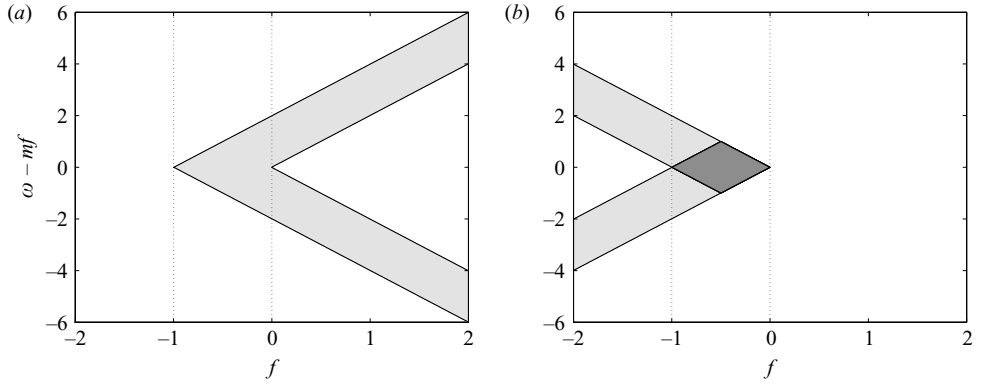

FIGURE 6. Frequency range of global Kelvin modes as a function of the Coriolis parameter, as predicted by the asymptotic theory. (*a*) $m=0$, $N=0$; (*b*) $m=0$, large N. Light grey, core modes; dark grey: ring modes.

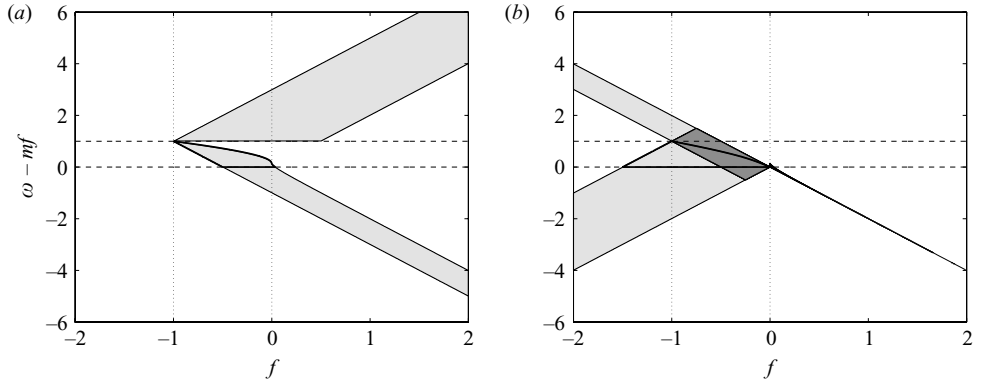

FIGURE 7. Same as figure 6 for (*a*) $m=1$, $N=0$; (*b*) $m=1$, large N. The horizontal dashed lines delimit the parameter region for which a critical-layer singularity is present. The thick solid lines delimit global mode regions of negative energy in (*a*) and of positive energy in (*b*).

horizontal lines located at $\omega - mf = 0$ and $\omega - mf = m$ delimit the frequency interval where a critical-point singularity is present. The plots of figures 6 to 9 have to be compared to the plots for the local frequencies (figures 2 and 3). As expected, global frequencies are within the local frequency domains. Moreover, frequencies of core modes are also within the domain of the local frequencies calculated in the vortex centre (pale grey regions in figures 2 and 3). However, the domain of global frequencies is much smaller than the domain of local frequencies. This demonstrates that the condition of existence of a global Kelvin mode is very restrictive.

We shall see in the next section (see figure 13*a*, *b*) that some of the global modes can possess a scattered wave structure. This occurs when the eigenmode is oscillating both in a finite interval (in which the eigenfrequency is selected) and in a semi-infinite interval extending to infinity. Le Dizès & Billant (2007) show that this scattering property is analogous to the radiative property of the bounded states of an atom. Here, it is easy to determine when scattering is present: the condition of scattering is that the radial wavenumber is real at $+\infty$. For non-stratified fluids, this happens when $-2|f| < \omega - mf < 2|f|$. The scattered wave is in that case an inertial wave. For strongly stratified fluids, scattering happens in the intervals $\omega - mf > 2|f|$

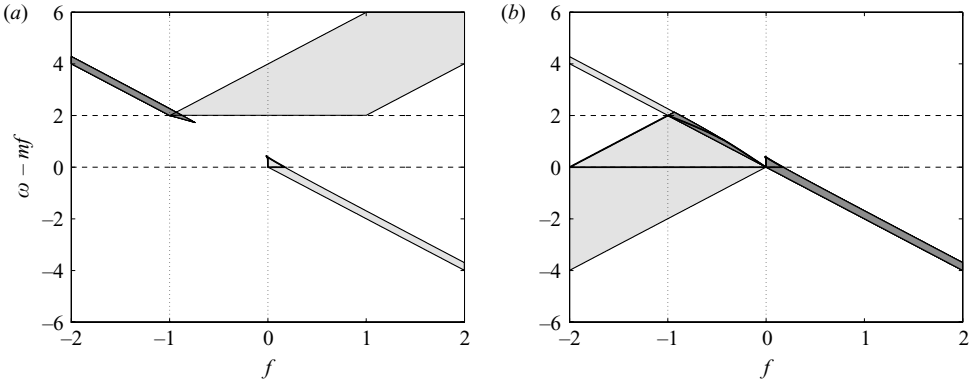

FIGURE 8. Same as figures 6 and 7 for (*a*) $m=2$, $N=0$; (*b*) $m=2$, large N.

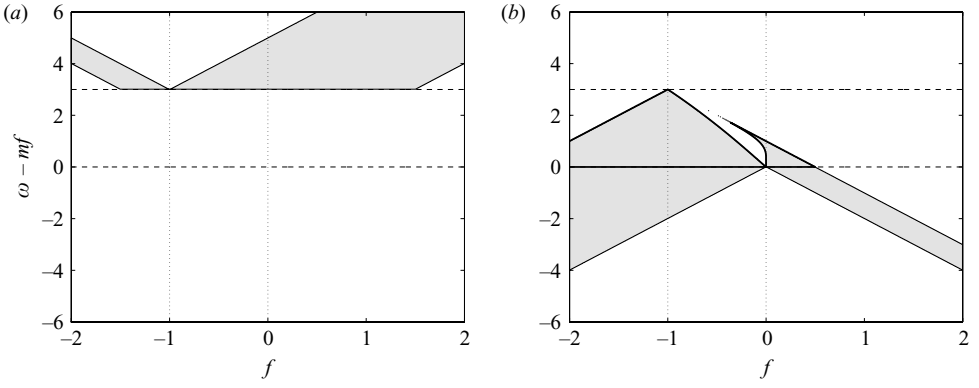

FIGURE 9. Same as figures 6 and 7 for (*a*) $m=3$, $N=0$; (*b*) $m=3$, large N.

or $\omega - mf < -2|f|$. The scattered wave is in that case a gravity wave. In general, this scattering phenomenon is (slightly) stabilizing. Yet, for the strongly stratified case, it can also become (slightly) destabilizing (see Le Dizès & Billant 2007).

For the elliptic instability we shall discuss below, it is also useful to define the energy of the global Kelvin mode in the rotating frame. As explained by Cairns (1979), the mode energy can be obtained from the dispersion relation $D(k_z, \omega)=0$ of the global Kelvin mode by a formula of the form

$$E = \tfrac{1}{4}(\omega - mf)\frac{\partial D}{\partial \omega} \times (\text{wave amplitude})^2. \tag{3.9}$$

Here, in the WKBJ framework, we have a simple expression for the dispersion relation (see (3.5) and (3.6)) such that the sign of the mode energy is given by the sign of

$$E_r = (\omega - mf)\int_I \frac{\left(\Delta_f + \Phi_f^2 - N^2\right)\Phi_f}{|\Delta_f|^{1/2}\left|\Phi_f^2 - N^2\right|^{3/2}}, \tag{3.10}$$

where the interval I is $(0, r_1)$ for the core modes, and (r_1, r_2) for the ring modes. It is worth mentioning that the above expression does not depend on the wavenumber k_z: all the global Kelvin modes of the same frequency and azimuthal wavenumber

have therefore the same energy sign. Expression (3.10) shows that in the unstratified case ($N=0$) or in the strongly stratified case (large N) the sign of the energy depends only on the signs of $(\omega - mf)$ and of Φ_f in the interval I. If both are positive, the energy of the mode is positive in the unstratified case, but negative in the strongly stratified case. Thus, we can easily deduce that in the unstratified case, all the modes have a positive energy except for $m=1$ when $0<\omega - mf<1$ and for $m=2$ when $0<\omega - mf<0.4$. (Naturally, there are symmetric intervals for negative m.) These negative energy modes are within the domains delimited by the thick solid lines in figures 7(*a*) and 8(*a*). In the strongly stratified case, it is the opposite: all the modes have a negative energy except some modes whose frequency is in the critical-layer interval. These positive energy modes are within the domains delimited by the thick solid lines in figures 7(*b*), 8(*b*) and 9(*b*).

In the next section, we analyse the consequences of these results on the elliptic instability of the Lamb–Oseen vortex when the latter is placed in a strain field rotating with the background flow. We obtain new conditions for the occurrence of the elliptic instability which could not have been obtained by the local approach.

4. Consequences on the elliptic instability

The elliptic instability can become active when the vortex is elliptically distorted by a background strain field. Here, we shall assume that this strain field is stationary in the rotating frame. Rotating strain field can be treated by a similar method.

If the strain field is weak, the elliptic instability can be analysed by a perturbation approach: the modification induced by the strain field is considered as a small disturbance of azimuthal wavenumber $m=2$. The elliptic instability mechanism can then be described by both a local and a global approach.

Locally, the strain disturbance acts on a Lagrangian particle as a temporal forcing of frequency $\omega_f = 2\Omega_0(r)$. This temporal forcing can resonantly couple two local plane waves if the difference between their local frequencies $\omega_l^{(1)}$ and $\omega_l^{(2)}$ differ by ω_f. Moreover, these two waves must also possess the same wavevector, that is the same $\cos\theta$. This implies that the condition of local resonance is $\omega_l^{(1)} = -\omega_l^{(2)} = \Omega(r)$. On a given radial location r, this condition is not satisfied for all f. We can easily show that in the strongly stratified case, f must be within an interval $(f_-(r), f_+(r))$ where

$$f_\pm(r) = -\left(\Omega_0(r) + \tfrac{1}{4} r\Omega_0'(r)\right) \pm \sqrt{\tfrac{1}{4}\,\Omega_0^2(r) + \tfrac{1}{16}(r\Omega_0'(r))^2}, \tag{4.1}$$

and, in the unstratified case, f must be outside this interval. The functions $f_-(r)$ and $f_+(r)$ for the Lamb–Oseen vortex, together with the limit of the centrifugal instability region are plotted in figure 10. The consequences for the Lamb–Oseen vortex are the following: in the unstratified case, there always exists a streamline on which the condition of local resonance can be satisfied whatever f; in the strongly stratified case, the condition of local resonance can be satisfied somewhere only for $-3/2 < f < f_{max} \approx 0.036$. Moreover, in that case, if $-1/2 < f < f_{max}$, this condition is not satisfied in the vortex centre, but on a streamline located far from the centre.

The inviscid growth rate associated with a local plane wave resonance can be calculated by a perturbation method (see for instance Le Dizès 2000). Leblanc (2003) has provided the local growth rate for the resonance in the vortex centre. A similar expression can be obtained on any streamline, but we shall not continue in this direction. Instead, we now discuss the constraints on the elliptic instability obtained from the global approach.

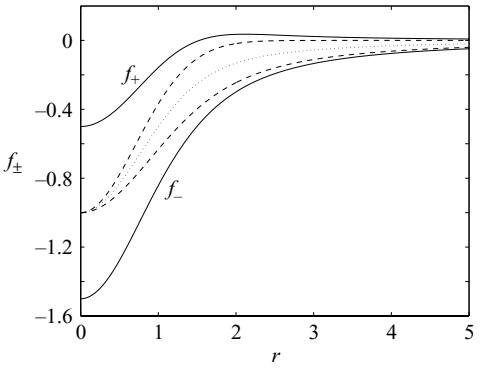

FIGURE 10. Variation of $f_\pm$ with respect to the radial coordinate r for a Lamb–Oseen vortex. Also indicated are the limits of the centrifugal instability region (dashed lines) and the most unstable Coriolis parameter $f_{max}(r)$ (dotted line).

In the global approach, the elliptic instability is also interpreted as a resonance phenomenon. Two global Kelvin modes are coupled through the correction induced by the strain field when their axial wavenumber, azimuthal wavenumber and frequency in the rotating frame satisfy

$$\omega_1 - m_1 f = \omega_2 - m_2 f, \tag{4.2a}$$

$$k_1 = k_2, \tag{4.2b}$$

$$m_1 = m_2 + 2. \tag{4.2c}$$

Using Cairns (1979), Fukumoto (2003) has argued that the resonance must also involve global Kelvin modes of opposite energy to imply instability. We have seen above that, in the WKBJ framework, the sign of the energy of the mode can easily be obtained. As neither the frequency domain nor the sign of the mode energy depend on the wavenumber, the condition of resonance can be examined by looking at the intersection of frequency domains of modes of azimuthal wavenumber m and $m+2$ and opposite energy sign. The result obtained by looking at these intersections is shown in figure 11 for the unstratified and the strongly stratified case. The labels indicate the azimuthal wavenumbers of the resonant global Kelvin modes. For instance, the solid line with the label $(-1, 1)$ in figure 11(a) delimits the region where a resonance between two modes $m=-1$ and $m=1$ of opposite energy is possible. All the possible resonances have been considered. The consequences of these plots are as follows.

(i) *In the unstratified case* (figure 11a): only the mode couples $(-1, 1)$ and $(0, \pm 2)$ can be resonantly excited by the strain field. Moreover, instability is possible only for a very limited range of Coriolis parameter: $-1/2 < f < f_{max} \approx 0.036$ for the $(-1, 1)$ resonance, $-0.016 < f < 0.09$ for the $(0, \pm 2)$ resonance. Note that except for the resonance of modes $(-1, 1)$ at $\omega - mf = 0$, one of the two resonant modes always possesses a critical-point singularity. This singularity is located far away from the region where the mode is localized and therefore has a very weak stabilizing effect.

(ii) *In the strongly stratified case* (figure 11b): only the couples $(-1, 1)$, $(0, \pm 2)$, $(\pm 1, \pm 3)$ and $(\pm 2, \pm 4)$ can be resonantly excited by the strain field. Except for the couples $(\pm 2, \pm 4)$ which are possibly unstable for $-3/2 < f < -0.45$ only, all the other couples can be unstable in the whole range $-3/2 < f < 0$. The mode couples $(-1, 1)$ can also be resonantly excited in a small interval of positive Coriolis parameters up to $f = f_{max} \approx 0.036$.

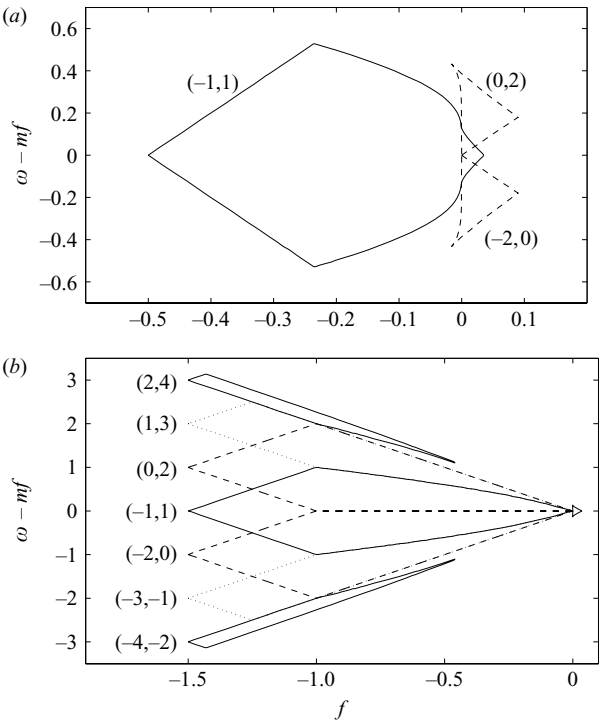

FIGURE 11. Domain in the $(f, \omega - mf)$-plane in which the elliptic instability is possible. The labels indicate the azimuthal wavenumbers of the global Kelvin modes involved in the resonance. (*a*) $N = 0$; (*b*) large N.

It is worth mentioning that for the strongly stratified case, the same unstable range of Coriolis parameter is obtained as in the local approach. By contrast, for the unstratified case, instability is predicted in a much smaller range of Coriolis parameter f. Local instability was expected whatever f, while here we have shown that instability is only possible in the interval $-1/2 < f < 0.09$.

The wavenumber of the resonant configurations can *a priori* be computed by searching the crossing points of two azimuthal branches m and $m + 2$ in the $(k_z, \omega - mf)$-plane. Because of a symmetry of the dispersion relation with respect to the transformation $(\omega, m) \rightarrow (-\omega, -m)$, some resonant points can be computed easily: they are the stationary modes of azimuthal wavenumber $m = 1$ which are automatically resonant with the stationary modes of azimuthal wavenumber $m = -1$. These two global Kelvin modes, owing to the symmetry, are perfectly in phase, such that their resonance is particularly efficient. When they have the same amplitude, their combination forms a sinuous mode which has been observed in several experiments (see Leweke & Williamson 1998; Afanasyev 2002; Meunier & Leweke 2005; Stegner *et al.* 2005). Theoretical arguments have also been provided to explain why they should be the most unstable (Le Dizès 2000; Le Dizès & Laporte 2002).

Here, the characteristics of these particular resonant modes can be easily computed from the WKBJ expression (3.5) or (3.6) of the dispersion relation. The results are shown in figure 12 for the unstratified case and a strongly stratified case ($N = 5$). As above, the agreement between the asymptotic results and the numerics is very good. In the unstratified case, the stationary sinuous modes are core modes. Their

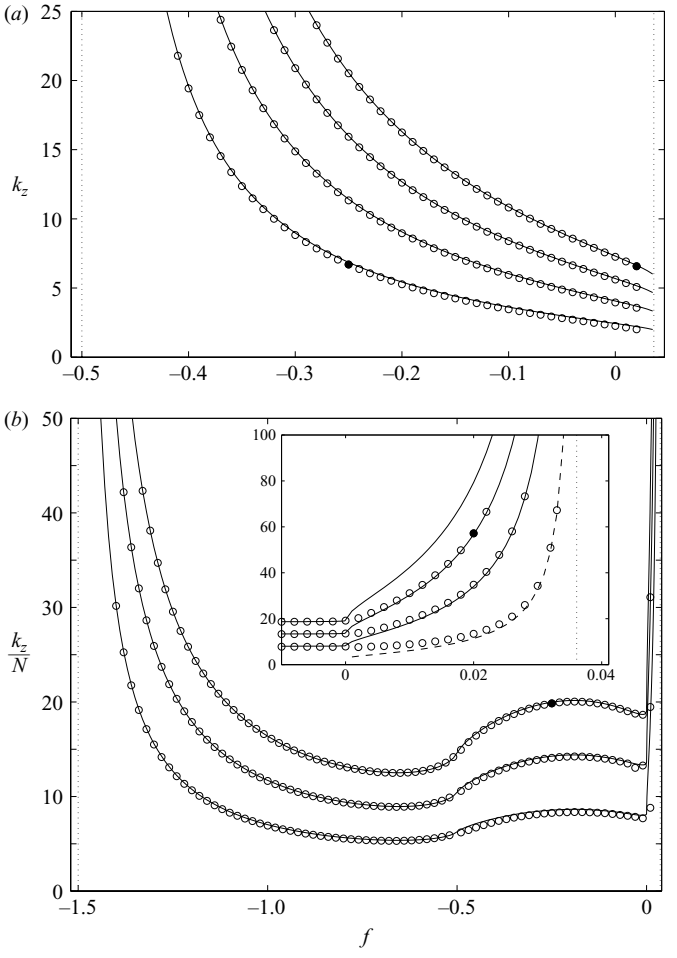

FIGURE 12. Variation of the axial wavenumber of the first stationary sinuous modes of the elliptical instability. (*a*) $N=0$; (*b*) $N=5$. WKBJ theory, solid and dashed lines; numerics, symbols. The dashed line corresponds to the branch with $n=0$ in the WKBJ formula. The eigenmodes associated with black symbols are represented in figure 13.

wavenumbers diverge as f tends to $-1/2$. It is important to recall that the centrifugal instability is active for negative f. The characteristics of the sinuous modes are thus expected to be relevant from an experimental point-of-view only for the largest value of f: for positive f when the vortex is stable with respect to the centrifugal instability or for small negative f when the centrifugal instability may not be sufficiently strong to dominate the elliptical instability.

In the strongly stratified case, the stationary sinuous modes are core modes for $-3/2 < f < -1/2$ and ring modes for $-1/2 < f < 0.036$. Again, the wavenumbers diverge for the smallest value of f. What is surprising, however, is the very rapid variation of the wavenumber for positive f. Note also the branch switching near $f=0$: the numerical results move from the branch $n+1$ to the branch n (n is the index appearing in (3.5) and (3.6)) as f changes from negative to positive. In particular, the branch $n=0$ exists for positive f, but not for negative f. In figure 12(*b*),

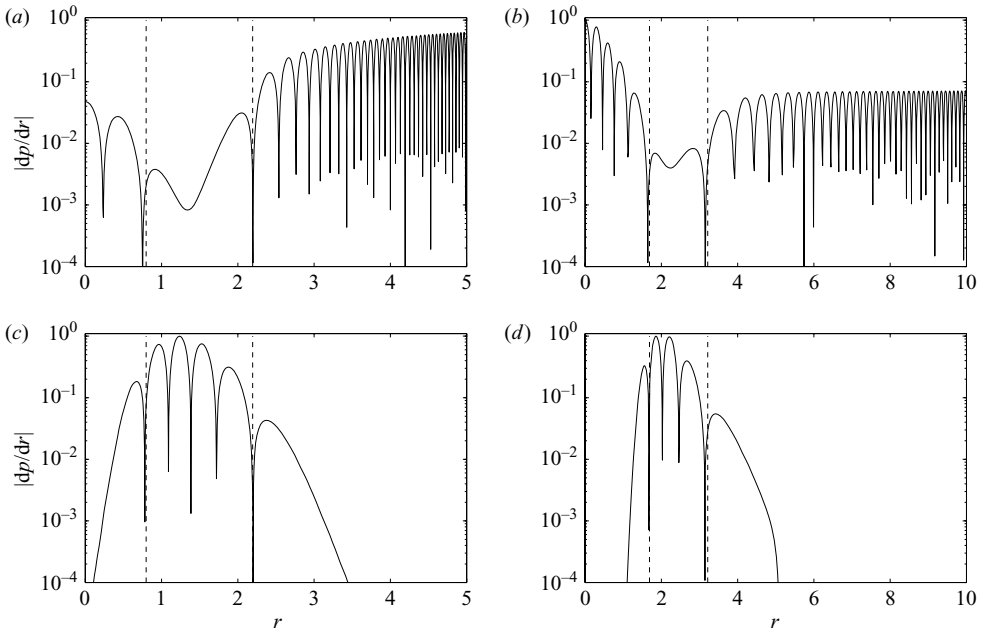

FIGURE 13. Typical variations versus r of the pressure derivative amplitude of the sinuous modes ($m=1$, $\omega=f$) obtained by numerical integration. The vertical dashed lines indicate the position of the turning points as predicted by the WKBJ theory. (*a*) $k=6.70$, $f=-0.25$, $N=0$; (*b*) $k=6.57$, $f=0.02$, $N=0$; (*c*) $k/N=19.85$, $f=-0.25$, $N=0$; (*d*) $k/N=57.15$, $f=0.02$, $N=5$.

a particular value of N has been considered. We have tried other values of N and observed that the results are almost invariant with respect to N as soon as $N>1$.

In both figures 12(*a*) and 12(*b*), we have not plotted the particular sinuous mode of zero wavenumber. This two-dimensional mode exists for all f in both the unstratified case and the strongly stratified case. It corresponds to the translation mode which intervenes in the zigzag instability (Billant & Chomaz 2000*a*). It cannot be captured by the WKBJ approach.

It is worth mentioning that the sinuous modes in the unstratified case have a specific structure (except when $f=0$): their eigenmode has an oscillating radial structure far from the vortex as illustrated in figures 13(*a*) and 13(*b*). In these plots is displayed the radial structure of the first eigenmode ($n=1$) for $f=-0.25$ (figure 13*a*), and of the fourth eigenmode ($n=4$) for $f=0.02$. The location of the turning points where the spatial structure is expected to change from evanescent to oscillatory is also shown. In the core region (between the origin and the first turning point), the eigenmode is oscillatory and possesses one zero in figure 13(*a*) and four zeros in figure 13(*b*) in agreement with the indexes $n=1$ and $n=4$ of the branch of the dispersion relation in each case, respectively. The eigenmode is also oscillatory after the second turning point. As already discussed in § 3, this oscillatory structure far from the vortex corresponds to the scattering of an inertial wave. This phenomenon is slightly stabilizing. For the mode shown in figure 13(*b*), the damping rate is -0.008.

In figures 13(*c*) and 13(*d*) are shown two sinuous modes in the strongly stratified case ($N=5$, here) corresponding to $f=-0.25$ and $f=0.02$, respectively. In both

cases, the eigenmodes are ring modes localized between two turning points. We can check that the number of zeros of the eigenmode corresponds to the branch label: $n=3$ in figure 13(c) and $n=2$ in figure 13(d). However, contrarily to the unstratified case, there is no scattering in those cases.

Afanasyev (2002) has analysed experimentally the stability of a vortex pair in a rotating unstratified environment corresponding to values of f in the intervals $(-1.5, -0.1)$ and $(0.1, 1.5)$. He found that only the anticyclonic vortex was destabilized. When the vortex was weakly deformed (the starting vortex) the centrifugal instability was active for f ranging from -1 to -0.3. When the vortex was strongly deformed (the stopping vortex), he found that the elliptic instability was the dominant feature. He observed the sinuous mode for f ranging from $-1/2$ to $-1/6$. These experimental observations are perfectly in agreement with our analysis. Afanasyev (2002) also measured the instability wavelength, but unfortunately he did not measure the characteristic radius of the vortices which would have permitted us to plot his data in figure 12(a). Yet, we can note that the growth of the sinuous mode wavelength he observed for increasing f is in agreement with the theory. Stegner *et al.* (2005) observed the elliptic instability in the anticyclonic vortices of a rotating von-Kármán vortex street and obtained the same qualitative features as Afanasyev (2002). However, none of these authors has reported the peculiar wave scattering structure of the instability modes. It would be interesting to determine whether these scattered waves are present in the experiments. Both Afanasyev (2002) and Stegner *et al.* (2005) reported elliptic instability for $-1 < f < -1/2$ which cannot be justified by the present theory. This extension of the elliptic instability domain is probably due to the large strain fields. It is also worth noting that centrifugal instability is active for these Coriolis parameters and that the unstable modes of the centrifugal instability are expected to be localized in the vortex core (see figure 1b: $r^{max} < 1$ for $f < -1/2$). Interaction with centrifugal instability could thus also provide an explanation for the elliptic instability for $f < -1/2$. This would be in agreement with the observations by Afanasyev (2002) who noticed that the instability characteristics are different from the classical elliptical instability in that Coriolis parameter range.

Experiments in a strongly stratified medium have been performed by Billant & Chomaz (2000a) and Otheguy *et al.* (2006b) for counter-rotating and co-rotating vortex pairs. Unfortunately, they only observed the zigzag instability and were not able to see the elliptic instability for the Froude and Reynolds numbers they considered. It would be interesting to perform new experiments in a fluid layer sufficiently thin to suppress the zigzag instability.

5. Conclusion

In this work, we have considered the local and global characteristics of inviscid waves on a Lamb–Oseen vortex in a rotating environment for an unstratified fluid and a strongly stratified fluid. We have first provided the local instability characteristics of the Lamb–Oseen vortex with respect to the centrifugal instability and shown that the local growth rate was superior to one tenth of the maximum angular velocity for the whole range of Coriolis parameter between -0.85 and -0.02. The characteristics of the global Kelvin modes have been analysed using a WKBJ approach. We have first shown by comparing typical asymptotic results with numerical results that our approximate dispersion relation can be trusted for small azimuthal wavenumbers. Our approach has permitted us to determine the frequency domains where global modes are expected as the Coriolis parameter is varied for azimuthal wavenumbers $m=0$

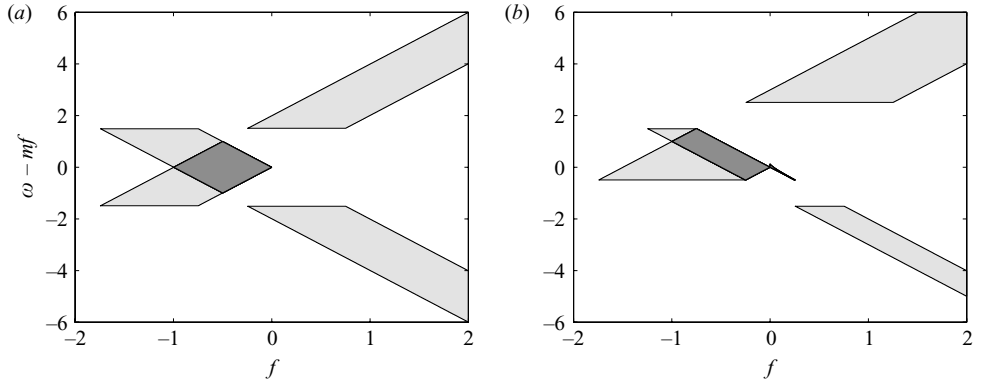

FIGURE 14. Frequency range of global Kelvin modes as a function of the Coriolis parameter for $N = 1.5$. (*a*) $m = 0$, (*b*) $m = 1$. Light grey, core modes; dark grey, ring modes.

to $m = 3$. We have shown that these domains are much smaller than the frequency domains of the local plane waves. The sign of the energy of the global modes has also been determined using the WKBJ approach.

These results have been discussed in the context of the elliptic instability and new necessary conditions for instability have been obtained. In particular, we have been able to demonstrate that the sinuous modes resulting from the coupling of the stationary helical modes $m = 1$ and $m = -1$ could be excited by the elliptic instability only if $-1/2 < f < 0.036$ in the unstratified case and only if $-3/2 < f < 0.036$ in the strongly stratified case. The variation of the wavenumbers of the first sinuous modes has been provided in these ranges.

Appendix A. Weakly stratified fluid

We have limited our analysis to either unstratified fluid or strongly stratified fluid. For weakly stratified fluid, the analysis is more complicated because of the presence of an additional critical-point singularity where the inertial frequency of the mode equals the Brunt–Väisälä frequency. Nevertheless, the WKBJ approach can still be used if we exclude the frequency intervals where such a critical point is present. This means, that the frequency intervals $(-N, -N + m)$ and $(N, N + m)$ have to be discarded. For frequencies smaller than $-N$ or larger than $N + m$, the global mode domains are then given by the analysis for an unstratified fluid. For frequencies in the interval $(-N + m, N)$ (if not empty), the global mode domains are given by the analysis for a strongly stratified fluid. To illustrate the method, we have provided in figure 14, the global mode domains obtained for $N = 1.5$ and for $m = 0$ (figure 14*a*) and $m = 1$ (figure 14*b*). Note that there is no critical-layer interval for $m = 0$ such that we jump directly from an unstratified configuration to a strongly stratified configuration as ω passes N. For $m = 1$ and $N = 1.5$, two frequency intervals $(-1.5, -0.5)$ and $(1.5, 2.5)$ where a critical layer exists are present. In these intervals, the global modes are expected to be damped by a mechanism similar to that in an unstratified fluid (see Schecter & Montgomery 2004; Fabre *et al.* 2006).

REFERENCES

AFANASYEV, Y. D. 2002 Experiments on instability of columnar vortex pairs in rotating fluid. *Geophys. Astrophys. Fluid Dyn.* **96**, 31–48.

Afanasyev, Y. D. & Peltier, W. R. 1998 Three-dimensional instability of anticyclonic swirling flow in rotating fluid: laboratory experiments and related theoretical predictions. *Phys. Fluids* **10**, 3194–3202.

Bayly, B. J. 1986 Three-dimensional instability of elliptical flow. *Phys. Rev. Lett.* **57**, 2160–2163.

Billant, P. & Chomaz, J.-M. 2000*a* Experimental evidence for a new instability of a vertical columnar vortex pair in a strongly stratified fluid. *J. Fluid Mech.* **418**, 167–188.

Billant, P. & Chomaz, J.-M. 2000*b* Theoretical analysis of the zigzag instability of a columnar vortex pair in a strongly stratified fluid. *J. Fluid Mech.* **419**, 29–63.

Billant, P. & Chomaz, J.-M. 2000*c* Three-dimensional stability of a vertical columnar vortex pair in a stratified fluid. *J. Fluid Mech.* **419**, 65–91.

Billant, P. & Gallaire, F. 2005 Generalized Rayleigh criterion for non-axisymmetric centrifugal instabilities. *J. Fluid Mech.* **542**, 365–379.

Billant, P., Chomaz, J.-M. & Otheguy, P. 2005 A general theory for the zigzag instability in stratified fluids. In *Intl Conf. on High Reynolds Number Vortex Interactions, Toulouse, France*, pp. 39–40.

Boubnov, B., Gledzer, E. & Hopfinger, E. 1995 Stratified circular Couette flow: instability and flow regimes. *J. Fluid Mech.* **292**, 333–358.

Cairns, R. A. 1979 The role of negative energy waves in some instabilities of parallel flows. *J. Fluid Mech.* **92**, 1–14.

Craik, A. D. D. 1989 The stability of unbounded two- and three-dimensional flows subject to body forces: some exact solutions. *J. Fluid Mech.* **198**, 275–292.

Crow, S. C. 1970 Stability theory for a pair of trailing vortices. *AIAA J.* **8**, 2172–2179.

Drazin, P. G. & Reid, W. H. 1981 *Hydrodynamic Stability*. Cambridge University Press.

Fabre, D., Sipp, D. & Jacquin, L. 2006 The Kelvin waves and the singular modes of the Lamb–Oseen vortex. *J. Fluid Mech.* **551**, 235–274.

Friedlander, S. & Lipton-Lifschitz, A. 2003 Localized instabilities in fluids. In *Handbook of Mathematical Fluid Dynamics* (ed. S. Fiendlander & D. Serre), vol. 2, pp. 289–354. North-Holland.

Fukumoto, Y. 2003 The three-dimensional instability of a strained vortex tube revisited. *J. Fluid Mech.* **493**, 287–318.

Kerswell, R. R. 2002 Elliptical instability. *Annu. Rev. Fluid Mech.* **34**, 83–113.

Kloosterziel, R. C. & van Heijst, G. J. F. 1991 An experimental study of unstable barotropic vortices in a rotating fluid. *J. Fluid Mech.* **223**, 1–24.

Lacaze, L., Ryan, K. & Le Dizès, S. 2007 Elliptic instability in a strained Batchelor vortex. *J. Fluid Mech.* **577**, 341–361.

Landau, L. & Lifchitz, E. 1967 *Mécanique Quantique, Théorie non relativiste*. Éditions MIR, Moscow.

Le Bars, M., Le Dizès, S. & Le Gal, P. 2007 Coriolis effects on the elliptical instability in cylindrical and spherical rotating containers. *J. Fluid Mech.* **585**, 323–342.

Le Dizès, S. 2000 Three-dimensional instability of a multipolar vortex in a rotating flow. *Phys. Fluids* **12** (11), 2762–2774.

Le Dizès, S. 2004 Viscous critical-layer analysis of vortex normal modes. *Stud. Appl. Maths* **112**, 315–332.

Le Dizès, S. & Billant, P. 2006 Instability of an axisymmetric vortex in a stably stratified fluid. In *6th European Fluid Mechanics Conference*, *Stockholm*, *Sweden*, p. 143.

Le Dizès, S. & Billant, P. 2007 Radiative instability in stratified vortices. *Phys. Rev. Lett.* (submitted).

Le Dizès, S. & Lacaze, L. 2005 An asymptotic description of vortex Kelvin modes. *J. Fluid Mech.* **542**, 69–96.

Le Dizès, S. & Laporte, F. 2002 Theoretical predictions for the elliptic instability in a two-vortex flow. *J. Fluid Mech.* **471**, 169–201.

Leblanc, S. 2003 Internal wave resonances in strain flows. *J. Fluid Mech.* **477**, 259–283.

Leweke, T. & Williamson, C. H. K. 1998 Cooperative elliptic instability of a vortex pair. *J. Fluid Mech.* **360**, 85–119.

Lifschitz, A. & Hameiri, E. 1991 Local stability conditions in fluid dynamics. *Phys. Fluids* A **3** (11), 2644–2651.

Meunier, P. & Leweke, T. 2005 Elliptic instability of a co-rotating vortex pair. *J. Fluid Mech.* **533**, 125–159.

Miyazaki, T. 1993 Elliptical instability in a stably stratified rotating fluid. *Phys. Fluids* A **5** (11), 2702–2709.

Miyazaki, T. & Fukumoto, Y. 1991 Axisymmetric waves on a vertical vortex in a stratified fluid. *Phys. Fluids* A **3**, 606–616.

Miyazaki, T. & Fukumoto, Y. 1992 Three-dimensional instability of strained vortices in stably stratified fluid. *Phys. Fluids* A **4**, 2515–2522.

Otheguy, P., Billant, P. & Chomaz, J.-M. 2006*a* The effect of planetary rotation on the zigzg instability of co-rotating vortices in a stratified fluid. *J. Fluid Mech.* **553**, 273–281.

Otheguy, P., Chomaz, J.-M. & Billant, P. 2006*b* Elliptic and zigzag instabilities on co-rotating vertical vortices in a stratified fluid. *J. Fluid Mech.* **553**, 253–272.

Saffman, P. G. 1992 *Vortex Dynamics*. Cambridge University Press.

Schecter, D. A. & Montgomery, M. T. 2004 Damping and pumping of a vortex Rossby wave in a monotonic cyclone: critical layer stirring versus inertia-buoyancy wave emission. *Phys. Fluids* **16**, 1334–48.

Sipp, D. & Jacquin, L. 2003 Widnall instabilities in vortex pairs. *Phys. Fluids* **15**, 1861–1874.

Staquet, C. & Sommeria, J. 2002 Internal gravity waves: from instabilities to turbulence. *Annu. Rev. Fluid Mech.* **34**, 559–593.

Stegner, A., Pichon, T. & Beunier, M. 2005 Elliptical–inertial instability of rotating Kármán streets. *Phys. Fluids* **17**, 066602.

Waleffe, F. 1990 On the three-dimensional instability of strained vortices. *Phys. Fluids* A **2** (1), 76–80.

Withjack, E. & Chen, C. 1974 An experimental study of Couette instability of stratified fluids. *J. Fluid Mech.* **66**, 725–737.